

Article

Comparative Study of ZnO Thin Films Doped with Transition Metals (Cu and Co) for Methylene Blue Photodegradation under Visible Irradiation

William Vallejo ^{1,*}, Alvaro Cantillo ¹, Brigitte Salazar ¹, Carlos Diaz-Uribe ¹, Wilkendry Ramos ¹, Eduard Romero ² and Mikel Hurtado ^{3,4}

¹ Photochemistry and Photobiology Research Group, College of Basic Sciences, Universidad del Atlántico, Puerto Colombia 81007, Colombia; acantilloguzman@mail.uniatlantico.edu.co (A.C.); bssalazar@mail.uniatlantico.edu.co (B.S.); carlosdiaz@mail.uniatlantico.edu.co (C.D.-U.); wramos@mail.uniatlantico.edu.co (W.R.)

² Department of Chemistry, College of Science, Universidad Nacional de Colombia, Bogotá 111321, Colombia; errromerom@unal.edu.co

³ Electronic Engineering College, Cluster NBIC, Universidad Central, Bogotá 111021, Colombia; mhurtadom1@ucentral.edu.co or mikel.hurtado@uniminuto.edu

⁴ Civil Engineering College, Universidad Minuto de Dios, Bogotá 110111, Colombia

* Correspondence: williamvallejo@mail.uniatlantico.edu.co; Tel.: +57-53599484

Received: 14 March 2020; Accepted: 6 May 2020; Published: 11 May 2020



Abstract: We synthesized and characterized both Co-doped ZnO (ZnO:Co) and Cu-doped ZnO (ZnO:Cu) thin films. The catalysts' synthesis was carried out by the sol-gel method while the doctor blade technique was used for thin film deposition. The physicochemical characterization of the catalysts was carried out by Raman spectroscopy, scanning electron microscopy (SEM), X-ray diffraction, and diffuse reflectance measurements. The photocatalytic activity was studied under visible irradiation in aqueous solution, and kinetic parameters were determined by pseudo-first-order fitting. The Raman spectra results evinced the doping process and suggested the formation of heterojunctions for both dopants. The structural diffraction patterns indicated that the catalysts were polycrystalline and demonstrated the presence of a ZnO wurtzite crystalline phase. The SEM analysis showed that the morphological properties changed significantly, the micro-aggregates disappeared, and agglomeration was reduced after modification of ZnO. The ZnO optical bandgap (3.22 eV) reduced after the doping process, these being ZnO:Co (2.39 eV) and ZnO:Cu (3.01 eV). Finally, the kinetic results of methylene blue photodegradation reached 62.6% for ZnO:Co thin films and 42.5% for ZnO:Cu thin films.

Keywords: thin films; ZnO; doping; heterogeneous photocatalysis

1. Introduction

Synthetic dyes are commonly used by various industries, especially textile ones. These physically and chemically stable compounds are harmful to the environment. Synthetic dyes are recalcitrant compounds that exhibit high solubility in water and accumulate in both wastewater and industrial effluents [1,2]. Currently, water pollution is one of the major challenges of the modern world, and the recovery of wastewater by conventional methods is not suitable for emergent pollutants [3,4]. Heterogeneous photocatalysis can be satisfactorily applied for the decontamination of natural samples through the photocatalytic degradation of toxic pollutants from complex matrices, such as river water and wastewater [5]. All renewable technologies have become a promising alternative for both energy generation and wastewater treatments. Solar photocatalysis is a suitable option to degrade recalcitrant

pollutants from water [6,7]. Different catalysts have been reported to exhibit photocatalytic activity (e.g., TiO₂ [8], Fe₂O₃ [9], ZnO [10], CuO [11], CdS [12], WO₃, and SnO₂ [13]). ZnO has been used as a photocatalyst, but its high bandgap value (~3.3 eV) is one of its major drawbacks. ZnO is not photocatalytically active at longer wavelengths of the electromagnetic spectrum. As a consequence, using solar irradiation as the main energy source to develop practical applications is a challenge for ZnO [14]. Some alternative strategies to extend ZnO photoresponse in the visible light region are: (a) ZnO doping [15–18], (b) co-doping [19,20], (c) coupling with lower band gap semiconductors [21,22], (d) surface plasmon resonance [23–26], (e) quantum dots [27], and (f) sensitization with natural and synthetic dyes [28–31]. With the doping process, optical and catalytic properties can be tuned by doping [32], and the ZnO bandgap generates intragap electronic states inside the semiconductor [33]. Some transition metals (e.g., Co²⁺, Ag⁺, Cu²⁺, Mn²⁺) have been used to enhance the properties of ZnO [34–37]. Among these, copper is an economical option. Because the ionic size of Cu²⁺ is close to Zn²⁺, Cu²⁺ ions can replace Zn²⁺ ions to modify the absorption spectrum [38]. Kuriakose et al. reported that Cu-doped ZnO nanostructures photodegraded organic dyes. Their analysis associated the enhanced photocatalytic activity to the combined effects of: (i) the separation of charge carriers and (ii) the optimal Cu doping load [39]. Another transition element is cobalt, as the ionic size of the Co²⁺ ion is close to that of Zn²⁺. Co²⁺ ions can replace Zn²⁺ and generate minimal distortion in the crystalline lattice [35,40]. Yongchun et al. reported the synthesis of cobalt-doped ZnO nanorods and reported an improvement in the performance of alizarin red photocatalytic degradation [41]. In addition, Kuriakose et al. synthesized Co-doped ZnO nanodisks and nanorods, and reported photocatalytic activity improvement as the by-effect of the doping process due to: (i) the charge separation efficiency and (ii) the surface area [42]. Poornaprakash et al. reported 66.5% efficiency in photocatalytic degradation of Rhodamine B under artificial solar light illumination on Co-doped ZnO nanorods [43]. The incorporation of these kinds of metals inside the ZnO structure can modify optical properties by extending the photodegradation ability towards the largest wavelength of the electromagnetic spectrum [44,45]. In this work, we report a facile wet chemical method for the synthesis of Cu and Co-doped ZnO thin films with highly enhanced photocatalytic activity. The metal doping process leads to highly efficient visible light photocatalytic degradation of methylene blue.

2. Results and Discussion

2.1. Structural Study

Figure 1 shows the XRD pattern for the catalysts synthesized in this study. The hexagonal wurtzite phase (JCPDS No. 36–1451) is identified as a crystalline structure for ZnO thin films, with the signals of the diffraction pattern corresponding to those reported by other authors [46]. The doping process did not affect the main signals in the diffraction patterns, as the XRD patterns for ZnO:Cu and ZnO:Co showed signals of a wurtzite ZnO structure. However, the XRD patterns showed a change in the intensity of the signals, suggesting that metal ions could substitute Zn²⁺ ions after the doping process. Lima et al. suggested that the change in the intensities could be associated with changes in both (i) grain size due to network defects and (ii) oxygen vacancies [47,48].

We used the Debye–Scherrer equation to calculate the crystalline domain size of the catalysts, using the full width at half maximum (FWHM) for the highest peak (101), with θ being the Scherrer diffraction angle [49]. Although there is no clear tendency between the intensity of the signal and metal doping load (see Figure 1b,c), all samples reduced the grain size of catalysis after the doping process (see Table 1). This could be explained by the incorporation of Co²⁺ and Cu²⁺ ions as dopants into the ZnO after the doping process [48,49]. Finally, the structural results suggest that ZnO films incorporated metallic ions. This observation was verified by Raman spectroscopy and diffuse reflectance, as described in the next sections.

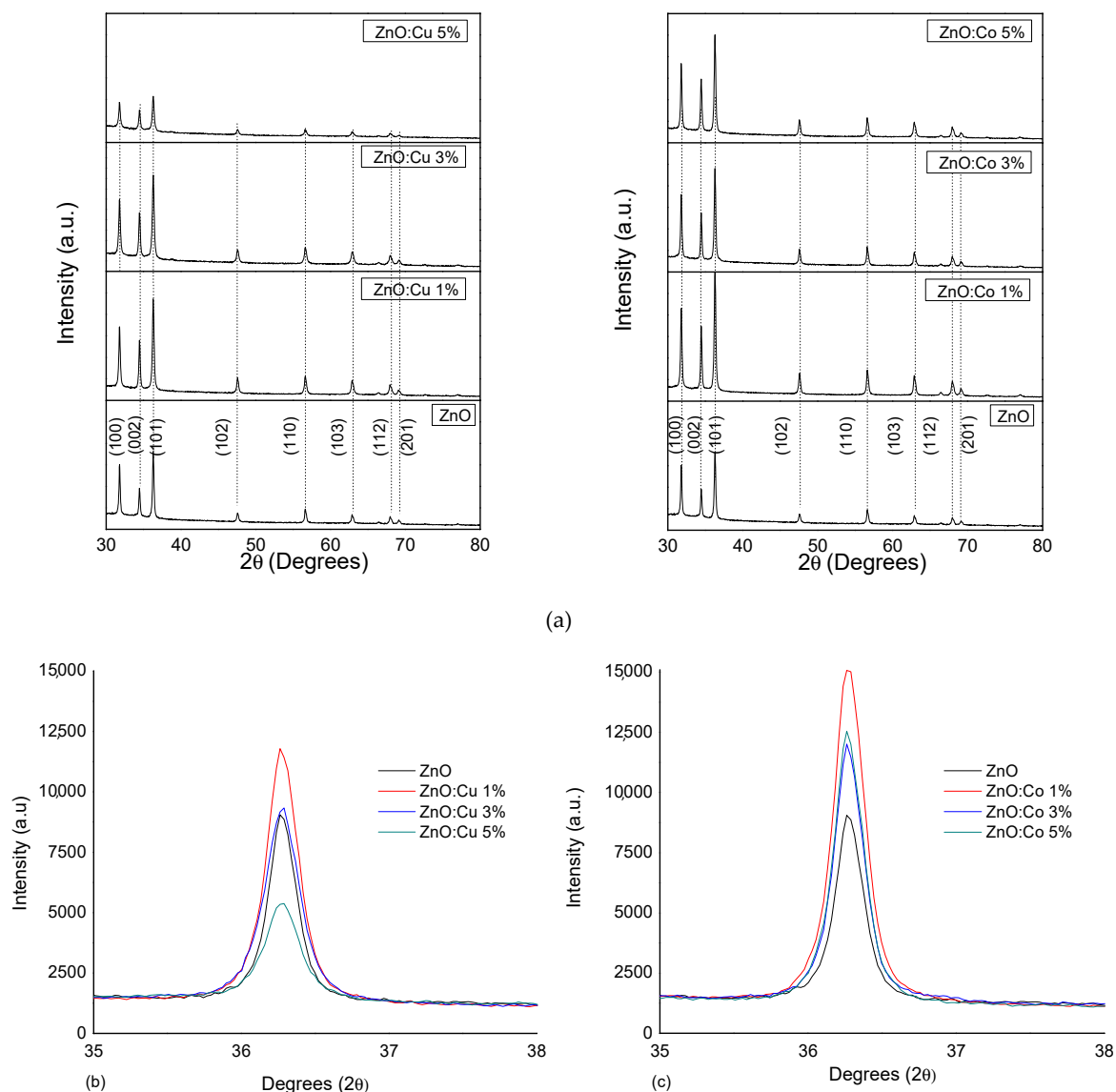


Figure 1. (a) X-ray diffraction patterns for the catalysts synthesized in this study. (b) Comparison of the highest peak (101) for ZnO:Cu. (c) Comparison of the highest peak (101) for ZnO:Co.

Table 1. Crystallographic results for the X-ray characterization of both undoped ZnO and metal-doped ZnO thin films.

Thin Film	FWHM * (101)	Intensity (101) Peak	Grain Size (nm)
ZnO	0.2396	8949	34.9
ZnO:Co 1%	0.2615	14,997	32.0
ZnO:Co 3%	0.2552	11,836	32.3
ZnO:Co 5%	0.2583	12,495	32.4
ZnO:Cu 1%	0.2601	11,649	32.1
ZnO:Cu 3%	0.2803	9202	29.8
ZnO:Cu 5%	0.3075	5300	27.2

* FWHM: full width at half maximum.

2.2. Raman Study

The Raman spectra of the catalysts are shown in Figure 2. All the peaks correspond with wurtzite-ZnO (C_{6v}^4): (i) 97.4 cm^{-1} (vibrational mode E_{2L}), (ii) 340 cm^{-1} ($E_{2H}-E_{2L}$), and (iii) 437.0 cm^{-1} and 581 cm^{-1} (A_1 vibrational mode) [50,51]. Figure 2a shows the Raman spectra for Cu-doped ZnO thin films. Signals E_{2L} ($\sim 99\text{ cm}^{-1}$) and E_{2H} ($\sim 437\text{ cm}^{-1}$) widen and decrease after the doping process—a behavior that can be explained by the incorporation of Cu^{2+} into the ZnO lattice. Additionally, this behavior has been associated with reduction of ZnO crystallinity by the formation of nanocomposites [52]. For greater Cu loads, Figure 2a shows two new signals, the first one located at 298 cm^{-1} and a second weak one at 614 cm^{-1} . These two signals can be attributed to modes A_{1g} and B_{2g} for CuO, respectively, and this result suggests the formation of a ZnO–CuO heterojunction during the synthesis process. The hydrodynamic stability of the suspension is affected by the concentration of reagents; so for obtaining greater Cu loads, the CuO generation is feasible. This result is in line with previous reports [39].

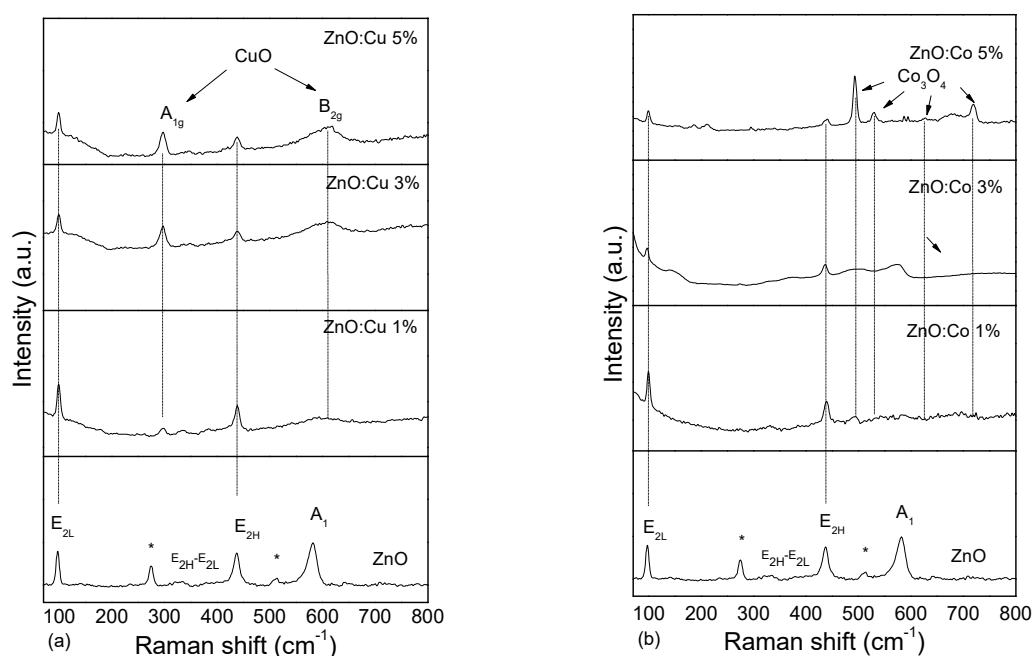


Figure 2. Raman spectra for: (a) ZnO:Cu and (b) ZnO:Co thin films. Inside the figures are the Raman vibration modes, where (*) corresponds to defects inside the ZnO structure.

Figure 2b shows the Raman spectrum for ZnO:Co; the intensity of A_{1LO} , E_{2L} , and E_{2H} modes decreases for these films. The ZnO:Co thin films (doping load 5%) show four new signals at 490 cm^{-1} , 526 cm^{-1} , 626 cm^{-1} , and 725 cm^{-1} . These signals could be attributed to the possible presence of Co_3O_4 , and these results confirm both the doping process and the formation of a heterojunction of ZnO– Co_3O_4 [53,54].

2.3. Morphological Study

Figure 3 shows SEM images for the catalysts. Figure 3a shows that the ZnO films formed microaggregates ($\sim 220\text{ nm}$) composed of quasi-spherical ZnO nanoparticles (around 40 nm in diameter), and this is a typical result for this material sensitized by the sol–gel method. Figure 3b,c shows that the morphological properties changed significantly after the doping process. Regarding the ZnO:Cu thin films, Figure 3b shows the formation of nanorods. Meanwhile, Figure 3c shows the formation of nanosized elongated particles of various shapes ($\sim 100\text{ nm}$) from the ZnO:Co thin films. Likewise, Figure 3c shows that the agglomeration on the catalyst surface reduced and the microaggregates

disappeared. Different nanostructures have been reported for ZnO (e.g., nanorods, nanotubes, nanobelts, nanosprings, nanospirals, nanorings) [55]. It is known that ZnO's morphological properties rely on synthesis conditions, and in our case, it is clear that the metal ions used during synthesis reduced the agglomeration and changed the thin films' morphology [56].

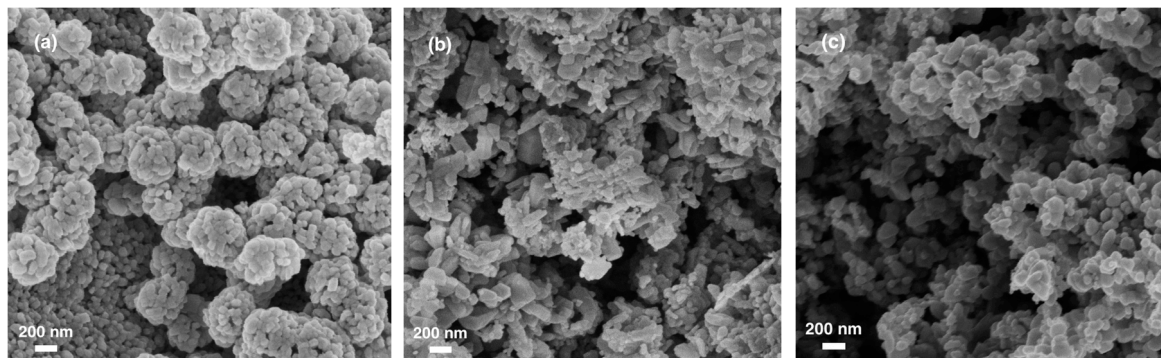


Figure 3. SEM images: (a) ZnO, (b) ZnO:Cu 5% and (c) ZnO:Co 5% thin films.

2.4. Optical Study

The diffuse reflectance spectra for the catalysts are shown in Figure 4. We used the Kubelka–Munk (KM) remission function for determining the bandgap energy value of the catalysts [57]. The use of the KM remission function makes it possible to obtain an analog to Tauc plots [58,59]:

$$(F(R_{\infty})hv)^{\frac{1}{2}} = A(hv - E_g) \quad (1)$$

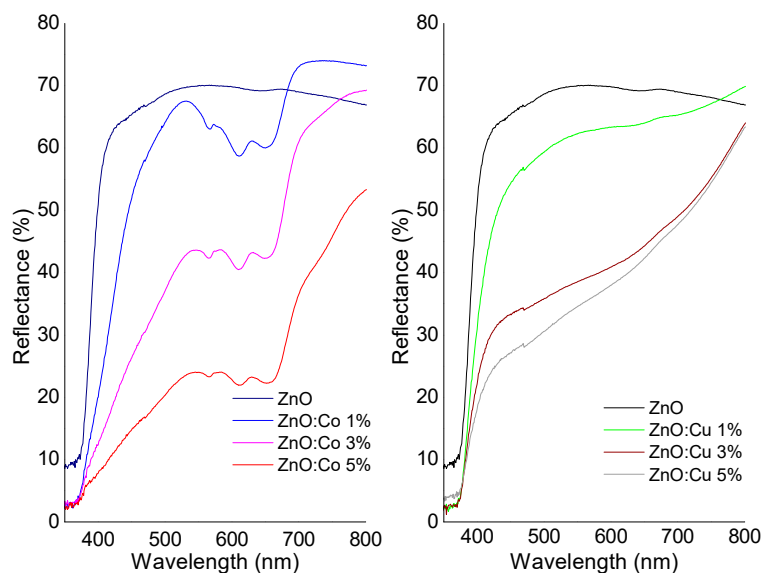


Figure 4. Reflectance diffuse spectra for both catalysts.

Figure 5 shows plots for $(F(R_{\infty})hv)^{\frac{1}{2}}$ versus (hv) and Table 2 lists the optical properties of the catalysts. Figure 5 shows that ZnO had a bandgap value (E_g) of 3.22 eV, a value that corresponds with that reported by Srikant et al. (3.1 eV and 3.2 eV) [60,61]. For doped ZnO catalysts, the E_g value was lower, and this behavior is associated with the reduction of the Fermi level of ZnO by the generation of intragap states. For ZnO:Cu, the modification of the bandgap can be attributed to the induction of 3d states of Cu located inside the bandgap of ZnO [37]. Additionally, the visible light absorption observed for doped ZnO can be attributed to intragap transitions between Cu 3d and

Zn 4s states. Furthermore, the ZnO:Co 5% catalyst has a lower bandgap value compared to other catalysts. This reduction is attributed to s-d and p-d exchange interactions between ZnO and Co^{2+} ions [62]. The 3d levels of Co^{2+} are located within the bandgap of ZnO, which can create new bands at larger wavelengths [63]. Some photoluminescence studies of the transition metal doping ZnO nanoparticles suggest that this important reduction in E_g value is due to oxygen deficiency [64]. Finally, the formation of nanoheterojunctions in the catalyst surface leads to an enhanced separation of charge carriers, increasing photocatalytic efficiency in addition to the doping process. The generation of these heterostructures has been reported for photocatalytic applications [65].

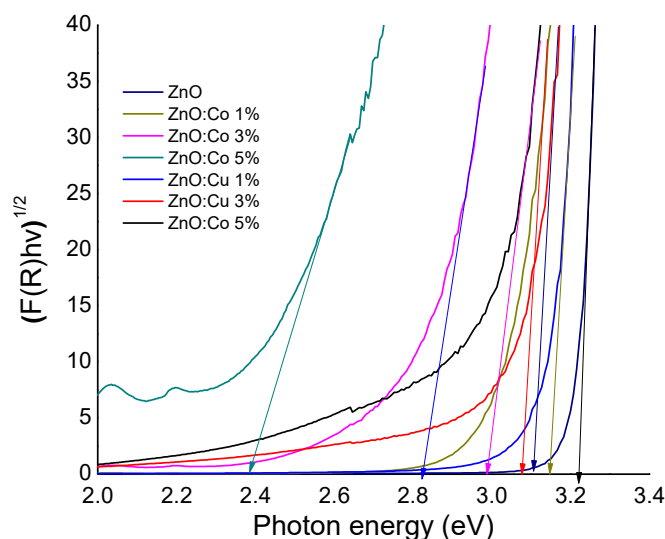


Figure 5. Kubelka–Munk (KM) fitting for the catalysts synthesized in this study.

Table 2. Band gap and results of pseudo-first-order model fitting.

Catalyst	$k_{ap} \times 10^{-3} \text{ (min}^{-1}\text{)}$	Degradation (%)	Band Gap (eV)
ZnO	0.2	2.7	3.22
ZnO:Co 1%	2.6	30.4	3.17
ZnO:Co 3%	4.2	45.7	2.83
ZnO:Co 5%	7.2	62.6	2.39
ZnO:Cu 1%	3.4	36.2	3.12
ZnO:Cu 3%	3.4	37.7	3.07
ZnO:Cu 5%	4.0	42.5	3.01

2.5. Photocatalytic Study

Figure 6 shows the decrease of MB as a function of time for all tests performed under visible irradiation. The MB concentration did not change after 140 min under visible irradiation, verifying the stability of MB dye. Furthermore, ZnO films did not show photocatalytic activity under visible irradiation (<3%). This result is in accordance with the ZnO bandgap energy value, and this photocatalyst is active only under UV irradiation. The ZnO:Co 5% catalyst reported the highest photocatalytic activity. This result can be explained by the lower bandgap value of the ZnO:Co 5% catalyst compared to other catalysts. The ZnO:Cu catalysts showed less photocatalytic activity than the Co-doped ZnO films. Compared to the Co-doped ZnO films, the bandgap values of this catalyst did not change; however, the best photodegradation result for ZnO:Cu was 42.5%, a value greater than that obtained for the ZnO thin films. The combined effect of the doping process and the heterojunction can explain this behavior. The photodegradation kinetics of MB on catalysts were studied by using the pseudo-first-order model [66]:

$$v_{[MB]} = [MB]_0 e^{-k_{ap}t} \quad (2)$$

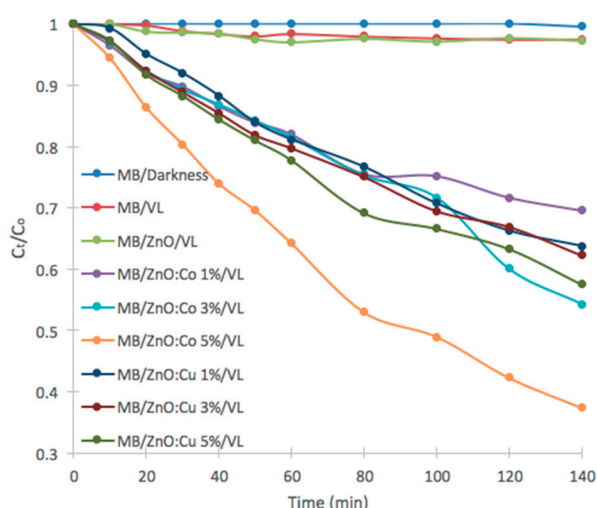


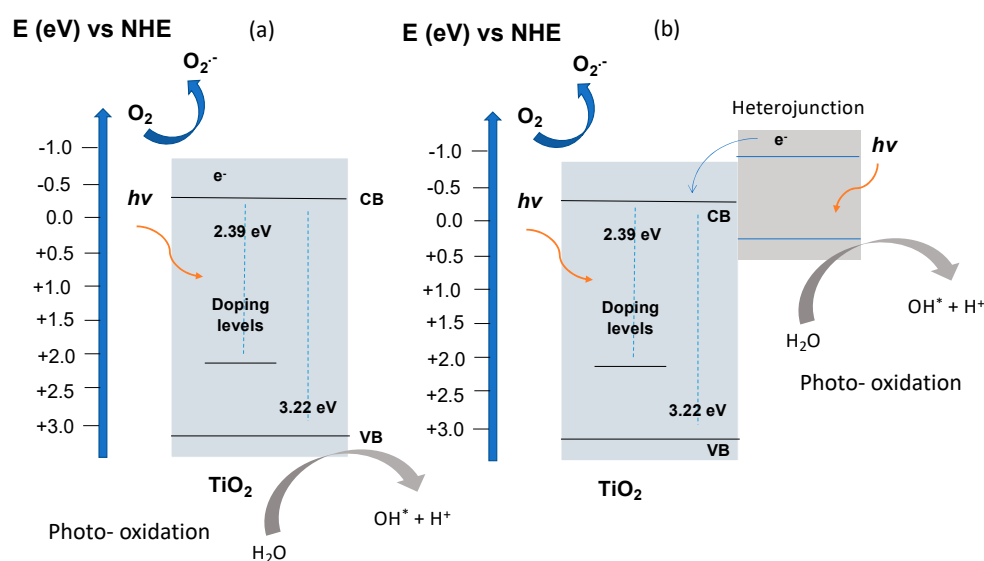
Figure 6. Methylene blue (MB) concentration vs. time of visible irradiation on the synthesized catalysts.

Time (t) is expressed in minutes and k_{app} is the apparent reaction rate constant (min^{-1}). Table 2 lists the kinetic parameters for the studied catalysts. Among all the catalysts, the ZnO thin films ($k_{app} = 0.2 \times 10^{-4} \text{ min}^{-1}$) showed the lowest k_{app} value, while the best results were obtained for ZnO:Co 5% ($k_{app} = 7.2 \times 10^{-3} \text{ min}^{-1}$) and ZnO:Cu 5% ($k_{app} = 4 \times 10^{-3} \text{ min}^{-1}$). In the best case, the kinetic rate constant was 36 times higher than the ZnO thin films. A combined effect could be present: (i) Cu doping in ZnO and (ii) the formation of a nanoheterojunction (ZnO–CuO). This synergic effect could be a reason for the increase in photocatalytic yields. The heterostructure generation for the methyl orange photodegradation under visible light irradiation has been reported before [67]. Table 3 lists other reports for the use of doped ZnO with different metals as catalysts. Our results indicate that the catalysts produced in this study are suitable options for solar photocatalytic applications.

Table 3. k_{app} values for different catalysts (ZnO doped with different metals) under visible irradiation.

Catalysts/Reference	Pollutant/Molar Concentration	Degradation (%) / Time Test	$k_{app} \times 10^{-3} (\text{min}^{-1})$
SnS/ZnO [67]	Rhodamine B/5 ppm	99%/175 min	21.2
	Methyl Orange/5 ppm	82%/125 min	13.9
Carbon-ZnO [68]	2,4-dinitrophenol/25 ppm	92%/140 min	18.3
ZnO:Co [41]	Alizarin Red/20 ppm	93%/60 min	—
ZnO:Cu [39]	Methyl Orange/5 ppm	80%/30 min	23
ZnO:Ag [69]	Methylene Blue/10 ppm	65%/140 min	4.1
ZnO:Co/this work	Methylene Blue/10 ppm	63%/140 min	7.2
ZnO:Cu/this work	Methylene Blue/10 ppm	43%/140 min	4.0

The ZnO films did not show photocatalytic activity under visible irradiation. However, two different processes can contribute to photocatalytic degradation under visible irradiation: (i) the intraband transitions as dopants allow the doped ZnO thin films to absorb visible light, generating charge pairs; (ii) CuO and Co_3O_4 can absorb visible light after the formation of ZnO–CuO and ZnO– Co_3O_4 heterojunctions, generating charge pairs. In this case, the electron can be transferred to the conduction band of ZnO. After electrons are located at the conduction band of ZnO, different reactive oxygen species (ROS) can be generated (e.g., O_2^- ; OH^\cdot), starting the MB photodegradation. Scheme 1 shows the general scheme of energetic levels for doped ZnO thin films and the ROS generation.



Scheme 1. Hypothetical scheme of energetic levels for metal-doped ZnO thin films: (a) Metal doping process. (b) Metal doping process and the generation of a heterojunction [64,70,71]. After charge pairs generation, the ROS can be yielded on the catalyst surface and MB degradation starts.

3. Materials and Methods

3.1. Synthesis and Characterization

The ZnO synthesis was carried out according to a previous report [69]: Twenty five mL of ammonium hydroxide (NH_4OH) (25–35% *w/w*) reactive grade (Merck) was placed in a 250 mL glass beaker, then 0.500 M ($\text{Zn}(\text{CH}_3\text{COO})_2 \cdot 2\text{H}_2\text{O}$) (Merck) was added dropwise at a rate of $1.7 \text{ mL} \cdot \text{min}^{-1}$ for 1 h, at a temperature of 85°C under constant agitation at 300 rpm. After that, the suspension stood for three days at room temperature then the solid was filtered and dried for 5 h at 100°C [72,73].

For the ZnO doping process, we used a similar procedure as previously described. While adding Zn^{2+} ions, we also added salts of the doping metals ($\text{CuSO}_4 \cdot 5\text{H}_2\text{O}$) (Merck) for copper doping and ($\text{Co}(\text{CH}_3\text{COO})_2 \cdot 4\text{H}_2\text{O}$) (JT Baker) for the cobalt doping processes. The synthesis of doped ZnO powder was performed at 1.0%, 3.0%, and 5.0%. The thin films were deposited using the doctor blade method, and the suspension was placed in a glass measuring 2 cm high and 2 cm wide. The thin films were heated for 30 min at 90°C to evaporate the solvent, and finally, the sintering process was performed at 500°C for 2 h [73,74]. Using this procedure, we obtained thin films ($6 \mu\text{m}$ thickness). The film thickness was measured through a Veeco Dektak 150 profilometer. The physical chemistry properties of the films were studied by X-ray diffraction, diffuse reflectance spectrophotometry, and Raman spectroscopy assay. X-ray diffraction patterns were obtained using a Shimadzu 6000 diffractometer using $\text{Cu K}\alpha$ radiation ($\lambda = 0.15406 \text{ nm}$) as an X-ray source with a diffraction angle in the 2θ range ($20\text{--}80^\circ$). Diffuse reflectance spectra were obtained with a Lambda 4 Perkin–Elmer spectrophotometer equipped with an integration sphere. The compositional properties of the materials were studied by Raman spectroscopy in a DXR device equipped with a 780 nm laser. The morphological properties were studied by scanning electron microscopy, under an excitation energy of 5 and 1 kV. The metallic content of the films was determined by plasma emission spectroscopy using the SM 3120 B technique, EPA 3015A modified for solids (see Supporting Information).

3.2. Photocatalytic Test

Methylene blue (MB) was chosen as the pollutant model in this study. The experiments were carried out in a batch reactor using an LED tape as a source of visible radiation (cold white light 17 watts), and the incident photon flow per unit volume I_0 was $5.8 \times 10^{-7} \text{ Einstein} \cdot \text{L}^{-1} \cdot \text{s}^{-1}$. Before irradiation,

the MB solution was kept in the dark for 90 min at 250 rpm to reach adsorption–desorption equilibrium on the catalysts' surface. Photodegradation was carried out using 50 ± 0.025 mL of an MB solution ($10 \text{ mg}\cdot\text{L}^{-1}$) saturated with oxygen at pH 7.0. The concentration of dye was determined through the spectrophotometric method (Thermo Scientific–Genesys 10S) using 665 nm as a fixed wavelength, with a calibration curve (correlation coefficient $R = 0.997$) for the use of the Lambert–Beer equation.

4. Conclusions

We synthesized and characterized ZnO thin films doped with Co and Cu. Raman results corroborated the doping process, which suggested the generation of a heterostructure. For the doped ZnO catalysts, the results show a reduction in the E_g values (from 3.22 to 2.42 eV for the best catalyst). This behavior is associated with a reduction of the Fermi level of ZnO by the presence of intragap states. The photocatalytic test indicated that doped catalysts had greater photocatalytic activity than unmodified catalysts, which could be attributed to (i) the generation of intraband states for the insertion of Co and Cu into ZnO, and (ii) the generation of ZnO–CuO and ZnO–Co₃O₄ heterojunctions. Furthermore, the rate of the photodegradation process (ZnO:Co 5%) was 36 times greater than the rate for unmodified ZnO, and the k_{app} values for the catalysts synthesized in this study had a suitable photocatalytic activity compared to other reports.

Supplementary Materials: The following are available online at <http://www.mdpi.com/2073-4344/10/5/528/s1>. Figure S1: ICP calibration curve for: (a) Co and (b) Cu content. Table S1: Results ICP for catalysts. Fitting curves of kinetic model.

Author Contributions: Conceptualization, W.V.; methodology, W.V., C.D.-U., B.S., A.C., W.R., E.R. and M.H.; validation, W.V., C.D.-U., B.S., A.C.; formal analysis, W.V., C.D.-U., B.S., A.C.; investigation, W.V., C.D.-U., B.S., A.C.; resources, W.V., C.D.-U., B.S., A.C., W.R., E.R. and M.H.; data curation, W.V., C.D.-U., B.S., A.C.; writing—original draft preparation, W.V., C.D.-U., B.S., A.C., writing—review and editing, W.V., C.D.-U., B.S., A.C., W.R., E.R., M.H.; visualization, W.V., C.D.-U.; supervision, W.V., C.D.-U.; project administration, W.V., C.D.-U.; funding acquisition, W.V., C.D.-U. All authors have read and agreed to the published version of the manuscript.

Funding: This research was funded by Universidad del Atlántico.

Acknowledgments: W.V., C.D.-U., B.S., and A.C. would like to thank Universidad del Atlántico.

Conflicts of Interest: The authors declare that there is no conflict of interest.

References

1. Lellis, B.; Fávaro-Polonio, C.Z.; Pamphile, J.A.; Polonio, J.C. Effects of textile dyes on health and the environment and bioremediation potential of living organisms. *Biotechnol. Res. Innov.* **2019**, *3*, 275–290. [[CrossRef](#)]
2. Hassan, M.M.; Carr, C.M. A critical review on recent advancements of the removal of reactive dyes from dyehouse effluent by ion-exchange adsorbents. *Chemosphere* **2018**, *209*, 201–219. [[CrossRef](#)]
3. Fabbri, D.; López-Muñoz, M.J.; Daniele, A.; Medana, C.; Calza, P. Photocatalytic abatement of emerging pollutants in pure water and wastewater effluent by TiO₂ and Ce-ZnO: Degradation kinetics and assessment of transformation products. *Photochem. Photobiol. Sci.* **2019**, *18*, 845–852. [[CrossRef](#)]
4. Zelinski, D.W.; dos Santos, T.P.M.; Takashina, T.A.; Leifeld, V.; Igarashi-Mafra, L. Photocatalytic Degradation of Emerging Contaminants: Artificial Sweeteners. *Water. Air. Soil Pollut.* **2018**, *229*, 1–12. [[CrossRef](#)]
5. Regulska, E.; Rivera-Nazarío, D.; Karpinska, J.; Plonska-Brzezinska, M.; Echegoyen, L. Zinc Porphyrin-Functionalized Fullerenes for the Sensitization of Titania as a Visible-Light Active Photocatalyst: River Waters and Wastewaters Remediation. *Molecules* **2019**, *24*, 1118. [[CrossRef](#)] [[PubMed](#)]
6. Ansari, S.A.; Ansari, S.G.; Foaud, H.; Cho, M.H. Facile and sustainable synthesis of carbon-doped ZnO nanostructures towards the superior visible light photocatalytic performance. *New J. Chem.* **2017**, *41*, 9314–9320. [[CrossRef](#)]
7. Naldoni, A.; Riboni, F.; Guler, U.; Boltasseva, A.; Shalaev, V.M.; Kildishev, A.V. Solar-Powered Plasmon-Enhanced Heterogeneous Catalysis. *Nanophotonics* **2016**, *5*, 112–133. [[CrossRef](#)]
8. Sedghi, R.; Heidari, F. A novel & effective visible light-driven TiO₂/magnetic porous graphene oxide nanocomposite for the degradation of dye pollutants. *RSC Adv.* **2016**, *6*, 49459–49468.

9. Balu, S.; Uma, K.; Pan, G.T.; Yang, T.C.K.; Ramaraj, S.K. Degradation of methylene blue dye in the presence of visible light using SiO₂@ α -Fe₂O₃ nanocomposites deposited on SnS₂ flowers. *Materials* **2018**, *11*, 1030. [[CrossRef](#)]
10. Loh, K.; Gaylarde, C.C.; Shirakawa, M.A. Photocatalytic activity of ZnO and TiO₂ ‘nanoparticles’ for use in cement mixes. *Constr. Build. Mater.* **2018**, *167*, 853–859. [[CrossRef](#)]
11. Saravanakumar, D.; Oualid, H.A.; Brahmi, Y.; Ayeshamariam, A.; Karunanaihy, M.; Saleem, A.M.; Kaviyarasu, K.; Sivaranjani, S.; Jayachandran, M. Synthesis and characterization of CuO/ZnO/CNTs thin films on copper substrate and its photocatalytic applications. *OpenNano* **2019**, *4*, 100025. [[CrossRef](#)]
12. Zyoud, A.; Zaatar, N.; Saadeddin, I.; Helal, M.H.; Campet, G.; Hakim, M.; Park, D.; Hilal, H.S. Alternative natural dyes in water purification: Anthocyanin as TiO₂-sensitizer in methyl orange photo-degradation. *Solid State Sci.* **2011**, *13*, 1268–1275. [[CrossRef](#)]
13. Elango, G.; Roopan, S.M. Efficacy of SnO₂ nanoparticles toward photocatalytic degradation of methylene blue dye. *J. Photochem. Photobiol. B Biol.* **2016**, *155*, 34–38. [[CrossRef](#)]
14. Das, A.; Malakar, P.; Nair, R.G. Engineering of ZnO nanostructures for efficient solar photocatalysis. *Mater. Lett.* **2018**, *219*, 76–80. [[CrossRef](#)]
15. Schumann, J.; Eichelbaum, M.; Lunkenbein, T.; Thomas, N.; Álvarez Galván, M.C.; Schlögl, R.; Behrens, M. Promoting Strong Metal Support Interaction: Doping ZnO for Enhanced Activity of Cu/ZnO:M (M = Al, Ga, Mg) Catalysts. *ACS Catal.* **2015**, *5*, 3260–3270. [[CrossRef](#)]
16. Kumari, V.; Mittal, A.; Jindal, J.; Yadav, S.; Kumar, N. S-, N- and C-doped ZnO as semiconductor photocatalysts: A review. *Front. Mater. Sci.* **2019**, *13*, 1–22. [[CrossRef](#)]
17. Bharat, T.C.; Mondal, S.; Gupta, H.S.; Singh, P.K.; Das, A.K. Synthesis of Doped Zinc Oxide Nanoparticles: A Review. *Mater. Today Proc.* **2019**, *11*, 767–775. [[CrossRef](#)]
18. Poornaprakash, U.; Chalapathi, K.; Subramanyam, S.V.; Prabhakar Vattikuti, Y.; Shun, S.P. Effects of Ce incorporation on the structural, morphological, optical, magnetic, and photocatalytic characteristics of ZnO nanoparticles. *Mater. Res. Express* **2019**, *6*, 105356. [[CrossRef](#)]
19. Poornaprakash, B.; Subramanyam, K.; Vattikuti, S.V.P.; Pratap Reddy, M.S. Achieving enhanced ferromagnetism in ZnTbO nanoparticles through Cu co-doping. *Ceram. Int.* **2019**, *45*, 16347–16352. [[CrossRef](#)]
20. Poornaprakash, B.; Chalapathi, U.; Poojitha, P.T.; Vattikuti, S.V.P.; Reddy, M.S.P. (Al, Cu) Co-doped ZnS nanoparticles: Structural, chemical, optical, and photocatalytic properties. *J. Mater. Sci. Mater. Electron.* **2019**, *30*, 9897–9902. [[CrossRef](#)]
21. Kaur, M.; Umar, A.; Mehta, S.K.; Singh, S.; Kansal, S.K.; Fouad, H.; Alothman, O.Y. Rapid Solar-Light Driven Superior Photocatalytic Degradation of Methylene Blue Using MoS₂-ZnO Heterostructure Nanorods Photocatalyst. *Material* **2018**, *11*, 2254.
22. Vallejo, W.; Díaz-Uribe, C.; Rios, K. Methylene Blue Photocatalytic Degradation under Visible Irradiation on In₂S₃ Synthesized by Chemical Bath Deposition. *Adv. Phys. Chem.* **2017**, *2017*, 1–5. [[CrossRef](#)]
23. Subash, B.; Krishnakumar, B.; Swaminathan, M.; Shanthi, M. Highly Efficient, Solar Active, and Reusable Photocatalyst: Zr-Loaded Ag-ZnO for Reactive Red 120 Dye Degradation with Synergistic Effect and Dye-Sensitized Mechanism. *Langmuir* **2013**, *29*, 939–949. [[CrossRef](#)] [[PubMed](#)]
24. Aby, H.; Kshirsagar, A.; Pk, K. Plasmon Mediated Photocatalysis by Solar Active Ag/ZnO Nanostructures: Degradation of Organic Pollutants in Aqueous Conditions. *J. Mater Sci Nanotechnol* **2016**, *4*. [[CrossRef](#)]
25. Díaz-Uribe, C.; Vilorio, J.; Cervantes, L.; Vallejo, W.; Navarro, K.; Romero, E.; Quiñones, C. Photocatalytic Activity of Ag-TiO₂ Composites Deposited by Photoreduction under UV Irradiation. *Int. J. Photoenergy* **2018**, *2018*, 1–8. [[CrossRef](#)]
26. Chen, L.; Tran, T.T.; Huang, C.; Li, J.; Yuan, L.; Cai, Q. Synthesis and photocatalytic application of Au/Ag nanoparticle-sensitized ZnO films. *Appl. Surf. Sci.* **2013**, *273*, 82–88. [[CrossRef](#)]
27. Poornaprakash, B.; Chalapathi, U.; Poojitha, P.T.; Vattikuti, S.V.P.; Park, S.H. Co-Doped ZnS Quantum Dots: Structural, Optical, Photoluminescence, Magnetic, and Photocatalytic Properties. *J. Supercond. Nov. Magn.* **2020**, *33*, 539–544. [[CrossRef](#)]
28. Youssef, Z.; Colombeau, L.; Yesmurzayeva, N.; Baros, F.; Vanderesse, R.; Hamieh, T.; Toufaily, J.; Frochot, C.; Roques-Carmes, T.; Acherar, S. Dye-sensitized nanoparticles for heterogeneous photocatalysis: Cases studies with TiO₂, ZnO, fullerene and graphene for water purification. *Dye. Pigment.* **2018**, *159*, 49–71. [[CrossRef](#)]

29. Vallejo, W.; Diaz-Uribe, C.; Cantillo, Á. Methylene blue photocatalytic degradation under visible irradiation on TiO₂ thin films sensitized with Cu and Zn tetracarboxy-phthalocyanines. *J. Photochem. Photobiol. A Chem.* **2015**, *299*, 80–86. [[CrossRef](#)]
30. Vallejo, W.; Rueda, A.; Díaz-Uribe, C.; Grande, C.; Quintana, P. Photocatalytic activity of graphene oxide–TiO₂ thin films sensitized by natural dyes extracted from *Bactris guineensis*. *R. Soc. Open Sci.* **2019**, *6*, 181824. [[CrossRef](#)]
31. Diaz-Uribe, C.; Vallejo, W.; Camargo, G.; Muñoz-Acevedo, A.; Quiñones, C.; Schott, E.; Zarate, X. Potential use of an anthocyanin-rich extract from berries of *Vaccinium meridionale* Swartz as sensitizer for TiO₂ thin films—An experimental and theoretical study. *J. Photochem. Photobiol. A Chem.* **2019**, *384*, 112050. [[CrossRef](#)]
32. Hamid, S.B.A.; Teh, S.J.; Lai, C.W. Photocatalytic Water Oxidation on ZnO: A Review. *Catalysts* **2017**, *7*, 93. [[CrossRef](#)]
33. Türkyılmaz, Ş.Ş.; Güy, N.; Özacar, M. Photocatalytic efficiencies of Ni, Mn, Fe and Ag doped ZnO nanostructures synthesized by hydrothermal method: The synergistic/antagonistic effect between ZnO and metals. *J. Photochem. Photobiol. A Chem.* **2017**, *341*, 39–50. [[CrossRef](#)]
34. Bouzid, H.; Faisal, M.; Harraz, F.A.; Al-Sayari, S.A.; Ismail, A.A. Synthesis of mesoporous Ag/ZnO nanocrystals with enhanced photocatalytic activity. *Catal. Today* **2015**, *252*, 20–26. [[CrossRef](#)]
35. Altintas Yildirim, O.; Arslan, H.; Sönmezoğlu, S. Facile synthesis of cobalt-doped zinc oxide thin films for highly efficient visible light photocatalysts. *Appl. Surf. Sci.* **2016**, *390*, 111–121. [[CrossRef](#)]
36. Ahmad, M.; Ahmed, E.; Ahmed, W.; Elhissi, A.; Hong, Z.L.; Khalid, N.R. Enhancing visible light responsive photocatalytic activity by decorating Mn-doped ZnO nanoparticles on graphene. *Ceram. Int.* **2014**, *40*, 10085–10097. [[CrossRef](#)]
37. Polat, İ.; Yılmaz, S.; Altın, İ.; Bacaksız, E.; Sökmen, M. The influence of Cu-doping on structural, optical and photocatalytic properties of ZnO nanorods. *Mater. Chem. Phys.* **2014**, *148*, 528–532. [[CrossRef](#)]
38. Mittal, M.; Sharma, M.; Pandey, O.P. UV-Visible light induced photocatalytic studies of Cu doped ZnO nanoparticles prepared by co-precipitation method. *Sol. Energy* **2014**, *110*, 386–397. [[CrossRef](#)]
39. Kuriakose, S.; Satpati, B.; Mohapatra, S. Highly efficient photocatalytic degradation of organic dyes by Cu doped ZnO nanostructures. *Phys. Chem. Chem. Phys.* **2015**, *17*, 25172–25181. [[CrossRef](#)]
40. Thennarasu, G.; Sivasamy, A. Metal ion doped semiconductor metal oxide nanosphere particles prepared by soft chemical method and its visible light photocatalytic activity in degradation of phenol. *Powder Technol.* **2013**, *250*, 1–12. [[CrossRef](#)]
41. Lu, Y.; Lin, Y.; Wang, D.; Wang, L.; Xie, T.; Jiang, T. A high performance cobalt-doped ZnO visible light photocatalyst and its photogenerated charge transfer properties. *Nano Res.* **2011**, *4*, 1144–1152. [[CrossRef](#)]
42. Kuriakose, S.; Satpati, B.; Mohapatra, S. Enhanced photocatalytic activity of Co doped ZnO nanodisks and nanorods prepared by a facile wet chemical method. *Phys. Chem. Chem. Phys.* **2014**, *16*, 12741. [[CrossRef](#)]
43. Poornaprakash, B.; Chalapathi, U.; Subramanyam, K.; Vattikuti, S.V.P.; Park, S.H. Wurtzite phase Co-doped ZnO nanorods: Morphological, structural, optical, magnetic, and enhanced photocatalytic characteristics. *Ceram. Int.* **2020**, *46*, 2931–2939. [[CrossRef](#)]
44. Rajbongshi, B.M.; Samdarshi, S.K. Cobalt-doped zincblende–wurtzite mixed-phase ZnO photocatalyst nanoparticles with high activity in visible spectrum. *Appl. Catal. B Environ.* **2014**, *144*, 435–441. [[CrossRef](#)]
45. Rajbongshi, B.M.; Samdarshi, S.K. ZnO and Co-ZnO nanorods—Complementary role of oxygen vacancy in photocatalytic activity of under UV and visible radiation flux. *Mater. Sci. Eng. B* **2014**, *182*, 21–28. [[CrossRef](#)]
46. Muchuweni, E.; Sathiaraj, T.S.; Nyakoty, H. Synthesis and characterization of zinc oxide thin films for optoelectronic applications. *Heliyon* **2017**, *3*, e00285. [[CrossRef](#)]
47. Yuhas, B.D.; Zitoun, D.O.; Pauzuskie, P.J.; He, R.; Yang, P. Transition-Metal Doped Zinc Oxide Nanowires. *Angew. Chemie* **2006**, *118*, 434–437. [[CrossRef](#)]
48. Wang, X.; Sø, L.; Su, R.; Wendt, S.; Hald, P.; Mamakhel, A.; Yang, C.; Huang, Y.; Iversen, B.B.; Besenbacher, F. The influence of crystallite size and crystallinity of anatase nanoparticles on the photo-degradation of phenol. *J. Catal.* **2014**, *310*, 100–108. [[CrossRef](#)]
49. Lima, M.K.; Fernandes, D.M.; Silva, M.F.; Baesso, M.L.; Neto, A.M.; de Moraes, G.R.; Nakamura, C.V.; de Oliveira Caleare, A.; Hechenleitner, A.A.W.; Pineda, E.A.G. Co-doped ZnO nanoparticles synthesized by an adapted sol–gel method: Effects on the structural, optical, photocatalytic and antibacterial properties. *J. Sol-Gel Sci. Technol.* **2014**, *72*, 301–309. [[CrossRef](#)]
50. Calleja, J.M.; Cardona, M. Resonant Raman scattering in ZnO. *Phys. Rev. B* **1977**, *16*, 3753–3761. [[CrossRef](#)]

51. Cuscó, R.; Alarcón-Lladó, E.; Ibáñez, J.; Artús, L.; Jiménez, J.; Wang, B.; Callahan, M.J. Temperature dependence of Raman scattering in ZnO. *Phys. Rev. B* **2007**, *75*, 165202. [[CrossRef](#)]
52. Wang, W.; Zhou, Q.; Fei, X.; He, Y.; Zhang, P.; Zhang, G.; Peng, L.; Xie, W. Synthesis of CuO nano- and micro-structures and their Raman spectroscopic studies. *CrystEngComm* **2010**, *12*, 2232. [[CrossRef](#)]
53. Winiarski, J.; Tylus, W.; Szczygieł, B. EIS and XPS investigations on the corrosion mechanism of ternary Zn–Co–Mo alloy coatings in NaCl solution. *Appl. Surf. Sci.* **2016**, *364*, 455–466. [[CrossRef](#)]
54. Xuan, H.; Yao, C.; Hao, X.; Liu, C.; Ren, J.; Zhu, Y.; Xu, C.; Ge, L. Fluorescence enhancement with one-dimensional photonic crystals/nanoscaled ZnO composite thin films. *Colloids Surfaces A Physicochem. Eng. Asp.* **2016**, *497*, 251–256. [[CrossRef](#)]
55. Hasnidawani, J.N.; Azlina, H.N.; Norita, H.; Bonnia, N.N.; Ratim, S.; Ali, E.S. Synthesis of ZnO Nanostructures Using Sol-Gel Method. *Procedia Chem.* **2016**, *19*, 211–216. [[CrossRef](#)]
56. Pourrahimi, A.M.; Liu, D.; Pallon, L.K.H.; Andersson, R.L.; Martínez Abad, A.; Lagarón, J.-M.; Hedenqvist, M.S.; Ström, V.; Gedde, U.W.; Olsson, R.T. Water-based synthesis and cleaning methods for high purity ZnO nanoparticles—comparing acetate, chloride, sulphate and nitrate zinc salt precursors. *RSC Adv.* **2014**, *4*, 35568–35577. [[CrossRef](#)]
57. Simmons, E.L. Relation of the Diffuse Reflectance Remission Function to the Fundamental Optical Parameters. *Opt. Acta Int. J. Opt.* **1972**, *19*, 845–851. [[CrossRef](#)]
58. Pal, M.; Pal, U.; Jiménez, J.M.G.Y.; Pérez-Rodríguez, F. Effects of crystallization and dopant concentration on the emission behavior of TiO₂:Eu nanophosphors. *Nanoscale Res. Lett.* **2012**, *7*, 1. [[CrossRef](#)]
59. Viezbicke, B.D.; Patel, S.; Davis, B.E.; Birnie, D.P. Evaluation of the Tauc method for optical absorption edge determination: ZnO thin films as a model system. *Phys. Status Solidi* **2015**, *252*, 1700–1710. [[CrossRef](#)]
60. Srikant, V.; Clarke, D.R. On the optical band gap of zinc oxide. *J. Appl. Phys.* **1998**, *83*, 5447–5451. [[CrossRef](#)]
61. El-Atab, N.; Chowdhury, F.; Ulusoy, T.G.; Ghobadi, A.; Nazirzadeh, A.; Okyay, A.K.; Nayfeh, A. ~3-nm ZnO Nanoislands Deposition and Application in Charge Trapping Memory Grown by Single ALD Step. *Sci. Rep.* **2016**, *6*, 38712. [[CrossRef](#)] [[PubMed](#)]
62. Liu, X.-C.; Shi, E.-W.; Chen, Z.-Z.; Zhang, H.-W.; Song, L.-X.; Wang, H.; Yao, S.-D. Structural, optical and magnetic properties of Co-doped ZnO films. *J. Cryst. Growth* **2006**, *296*, 135–140. [[CrossRef](#)]
63. Qiu, X.; Li, G.; Sun, X.; Li, L.; Fu, X. Doping effects of Co²⁺ ions on ZnO nanorods and their photocatalytic properties. *Nanotechnology* **2008**, *19*, 215703. [[CrossRef](#)] [[PubMed](#)]
64. Ramya, E.; Rao, M.V.; Jyothi, L.; Rao, D.N. Photoluminescence and Nonlinear Optical Properties of Transition Metal (Ag, Ni, Mn) Doped ZnO Nanoparticles. *J. Nanosci. Nanotechnol.* **2018**, *18*, 7072–7077. [[CrossRef](#)] [[PubMed](#)]
65. Xu, H.; Shi, M.; Liang, C.; Wang, S.; Xia, C.; Xue, C.; Hai, Z.; Zhuiykov, S. Effect of Zinc Acetate Concentration on Optimization of Photocatalytic Activity of p-Co₃O₄/n-ZnO Heterostructures. *Nanoscale Res. Lett.* **2018**, *13*, 195. [[CrossRef](#)]
66. Konstantinou, I.K.; Albanis, T.A. TiO₂—Assisted photocatalytic degradation of azo dyes in aqueous solution: Kinetic and mechanistic investigations A review. *Appl. Catal. B Environ.* **2004**, *49*, 1–14. [[CrossRef](#)]
67. Jayswal, S.; Moirangthem, R.S. Construction of a solar spectrum active SnS/ZnO p–n heterojunction as a highly efficient photocatalyst: The effect of the sensitization process on its performance. *New J. Chem.* **2018**, *42*, 13689–13701. [[CrossRef](#)]
68. Jun Park, S.; Sankar Das, G.; Schütt, F.; Adelung, R.; Kumar Mishra, Y.; Malika Tripathi, K.; Kim, T. Visible-light photocatalysis by carbon-nano-onion-functionalized ZnO tetrapods: Degradation of 2,4-dinitrophenol and a plant-model-based ecological assessment. *Asia Mater.* **2019**, *11*, 1–13.
69. Vallejo, W.; Cantillo, A.; Dias-Urbe, C. Methylene Blue Photodegradation under Visible Irradiation on Ag-Doped ZnO Thin Films. *Int. J. Photoenergy* **2020**, *2020*, 112. [[CrossRef](#)]
70. Prasad, C.; Tang, H.; Liu, Q.Q.; Zulfikar, S.; Shah, S.; Bahadur, I. An overview of semiconductors/layered double hydroxides composites: Properties, synthesis, photocatalytic and photoelectrochemical applications. *J. Mol. Liq.* **2019**, *289*, 111114. [[CrossRef](#)]
71. Hernández-Alonso, M.D.; Fresno, F.; Suárez, S.; Coronado, J.M. Development of alternative photocatalysts to TiO₂: Challenges and opportunities. *Energy Environ. Sci.* **2009**, *2*, 1231–1257. [[CrossRef](#)]
72. Pérez, J.A.; Gallego, J.L.; Wilson Stiven Roman, H.R.L. Zinc Oxide Nanostructured Thin Films. *Sci. Tech.* **2008**, *39*, 416–421.

73. Ramírez Vinasco, D.; Vera, L.; Patricia, L.; Riascos Landázuri, H. Zn_{1-x}Mn_xO Thin Films. *Sci. Tech.* **2009**, *41*, 273–278.
74. Quiñones, C.; Ayala, J.; Vallejo, W. Methylene blue photoelectrodegradation under UV irradiation on Au/Pd-modified TiO₂ films. *Appl. Surf. Sci.* **2010**, *257*, 367–371. [[CrossRef](#)]



© 2020 by the authors. Licensee MDPI, Basel, Switzerland. This article is an open access article distributed under the terms and conditions of the Creative Commons Attribution (CC BY) license (<http://creativecommons.org/licenses/by/4.0/>).